

Vulnerabilities in AI-generated Image Detection: The Challenge of Adversarial Attacks

Yunfeng Diao
Hefei University of Technology
Hefei, China

Naixin Zhai
University of Science and Technology
of China
Hefei, China

Changtao Miao
University of Science and Technology
of China
Hefei, China

Xun Yang
University of Science and Technology
of China
Hefei, China

Meng Wang
Hefei University of Technology
Hefei, China

ABSTRACT

Recent advancements in image synthesis, particularly with the advent of GAN and Diffusion models, have amplified public concerns regarding the dissemination of disinformation. To address such concerns, numerous AI-generated Image (AIGI) Detectors have been proposed and achieved promising performance in identifying fake images. However, there still **lacks a systematic understanding of the adversarial robustness of AIGI detectors**. In this paper, we examine the vulnerability of state-of-the-art AIGI detectors against adversarial attack under white-box and black-box settings, which has been rarely investigated so far. For the task of AIGI detection, we propose a new attack containing two main parts. First, inspired by the obvious difference between real images and fake images in the frequency domain, we add perturbations under the frequency domain to push the image away from its original frequency distribution. Second, we explore the full posterior distribution of the surrogate model to further narrow this gap between heterogeneous models, e.g. transferring adversarial examples across CNNs and ViTs. This is achieved by introducing a novel post-train Bayesian strategy that turns a single surrogate into a Bayesian one, capable of simulating diverse victim models using one pre-trained surrogate, without the need for re-training. We name our method as frequency-based post-train Bayesian attack, or FPBA. Through FPBA, we show that adversarial attack is truly a real threat to AIGI detectors, because FPBA can deliver successful black-box attacks across models, generators, defense methods, and even evade cross-generator detection, which is a crucial real-world detection scenario. The code will be shared upon acceptance.

CCS CONCEPTS

• **Security and privacy** → **Software and application security; Human and societal aspects of security and privacy;** • **Computing methodologies** → **Computer vision.**

Permission to make digital or hard copies of all or part of this work for personal or classroom use is granted without fee provided that copies are not made or distributed for profit or commercial advantage and that copies bear this notice and the full citation on the first page. Copyrights for components of this work owned by others than the author(s) must be honored. Abstracting with credit is permitted. To copy otherwise, or republish, to post on servers or to redistribute to lists, requires prior specific permission and/or a fee. Request permissions from permissions@acm.org.
Conference'17, July 2017, Washington, DC, USA

© 2024 Copyright held by the owner/author(s). Publication rights licensed to ACM.
ACM ISBN 978-x-xxxx-xxxx-x/YY/MM
<https://doi.org/10.1145/nnnnnnn.nnnnnnn>

KEYWORDS

AI-generated Image Detection, Adversarial Examples

ACM Reference Format:

Yunfeng Diao, Naixin Zhai, Changtao Miao, Xun Yang, and Meng Wang. 2024. Vulnerabilities in AI-generated Image Detection: The Challenge of Adversarial Attacks. In . ACM, New York, NY, USA, 10 pages. <https://doi.org/10.1145/nnnnnnn.nnnnnnn>

1 INTRODUCTION

The notable progress in generative models, such as GANs [18] and Diffusion models [22], is driving the flourishing development of the image synthesis domain. These generated fake images exhibit realistic-looking, rendering them visually indistinguishable from real images. Moreover, a variety of free and open-source tools facilitates the effortless creation of fake images. However, alongside the benefits, the widespread availability of fake images raises concerns regarding the dissemination of misinformation and fake media news.

Consequently, numerous detectors have been proposed [4, 8, 15] to identify AI-generated images (AIGI). Recent state-of-the-art detectors [55, 62] rely on Deep Neural Networks (DNNs) to classify, achieving significant accuracy performance across multiple datasets and generative models. However, our investigation reveals that AIGI detectors are vulnerable to adversarial examples, capable of misleading detectors by classifying fake images as real. Despite several works [3, 23, 25, 28, 44] exploring adversarial attacks for GAN-based face forgery detection, we extend this security issue to encompass broader AIGI detection, which has been largely ignored. Unlike face forgery concentrates solely on manipulating or synthesizing faces, often crafted by GANs, AI-generated images span a broader spectrum, generated by a variety of advanced diffusion models and GANs. These images encompass a richer array of semantic content, thus greatly enhancing their potential for disseminating disinformation.

In this paper, we show that AIGI detectors are vulnerable to adversarial attacks. Considering that many works [16, 17] have demonstrated the obvious changes between real and fake images in the frequency domain, we explore the vulnerable region of AIGI detectors in the frequency domain. As illustrated in Fig. 3, the frequency components that different detectors focus on significantly vary from each other. Therefore, we utilize frequency spectrum

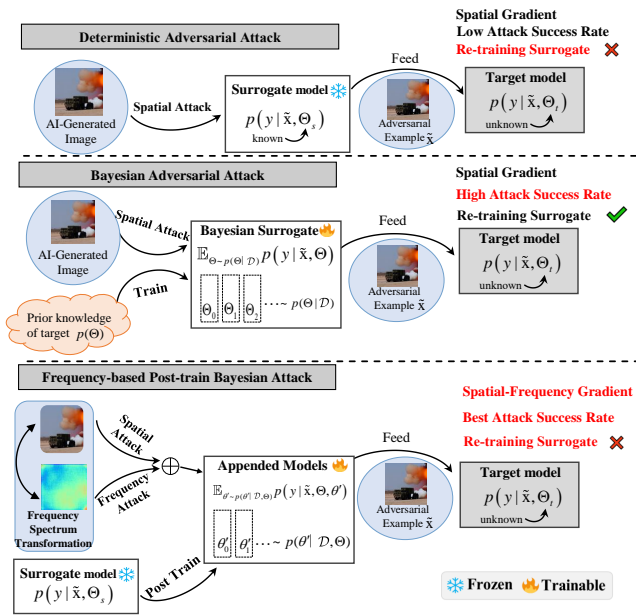


Figure 1: Illustration of the proposed method.

transformation to uncover diverse substitute models. To further improve the adversarial transferability across heterogeneous models, e.g. transferring adversarial examples across Visual Transformers (ViTs) and Convolutional Neural Networks (CNNs), we propose a post-train Bayesian strategy to conduct a Bayesian treatment on the surrogate model, without the need for re-training the surrogate. In contrast to existing ensemble-based or Bayesian attacks, which involve retraining an ensemble of surrogate models, our post-train Bayesian strategy freezes the pre-trained surrogate and appends tiny extra Bayesian components behind the surrogate, avoiding a heavy memory footprint and speeding up the training process. As a result, we propose the first adversarial attack for general AIGI detection, to add adversarial perturbations in the frequency domain from a post-train Bayesian perspective. We name our method Frequency-based Post-train Bayesian Attack, or FPBA. A high-level illustration of our method and the key differences between our method and the previous method are shown in Fig. 1.

The contributions of this work can be summarized as follows:

- To our best knowledge, we are the first to systemically investigate the adversarial vulnerability of state-of-the-art AIGI detectors. We extensively evaluate the adversarial robustness of traditionally trained models, defense models, and cross-generated detection within real-world scenarios. We demonstrate adversarial examples are truly a real threat to AIGI detections, and reveal the phenomenon of gradient masking phenomena in AIGI detectors.
- We propose a novel attack against AIGI detection by exploring the vulnerable frequency region in a Bayesian manner. A new post-train Bayesian strategy for attack is proposed to explore the full posterior distribution over the surrogate, without the need for re-training the substitute model.

- We conduct comprehensive experiments on eight spatial-based detectors with CNN-based, ViT-based and CLIP-based architectures, and two frequency-based detectors using AIGI and Deepfake datasets. The extensive results demonstrate our proposed method achieves the highest average attack success rate under white-box and black-box settings, outperforming baseline methods by a big margin.

2 RELATED WORK

AI-Generated Image Detection: The rapid advancement of AI generative technologies, including GANs [18], VAEs [33], and Diffusion models [22], has brought about substantial risks in the dissemination of disinformation. Initially, early VAEs and GANs models were primarily utilized to generate realistic fake face data, leading detection methods to primarily focus on face forgeries. However, with the emergence of diffusion models, the scope of generative models has expanded to encompass diverse natural scene objects. Consequently, this expansion presents more significant challenges to detection methods, as they must now address a broader range of forgery types and scenarios.

The primary objective of AIGI detection methods is to discern the authenticity of an image by framing it as a binary classification task, distinguishing between real and fake instances. Data-driven-based approaches [4, 8, 15, 55] have demonstrated promising results on generated data identically distributed. However, their performance significantly degraded when presented with previously unseen generated images. More recently, certain methods [5, 16, 17] focus on analyzing forgery traces in the frequency domain and learning relevant forgery features [7, 37, 46, 60] to enhance the generalization capability of the detection system. In pursuit of these objectives, some methods have been proposed to learn local forgery features [30, 41] in the spatial domain. AIGI fingerprint representations [27] are acquired through the learning of noise patterns. Notably, studies such as [36, 62] have demonstrated the utility of utilizing noise in the frequency domain as a fingerprint for enhancing performance. A sequence of detection methodologies [6, 9, 37, 52] has been progressively investigated, relying on the practice of freezing pre-trained models. These approaches employ parameter-efficient fine-tuning strategies while integrating additional classifiers. For instance, UniFD [45] explores pre-trained vision-language models for AIGI detection, showcasing the effectiveness of leveraging such models in the pursuit of robust forgery detection. Furthermore, other researchers have pursued a comprehensive investigation of generalized forgery features from various perspectives, ranging from diffusion reconstruction error [48, 56], adversarial teacher-student discrepancy-aware framework [63] or diffusion noise [61].

The existing models consistently demonstrate enhancement in detecting AI-generated images. However, their behaviors under adversarial attacks have not been thoroughly examined. Our work is complementary to existing research by making the first attempt to systemically evaluate their robustness to adversarial attacks and suggesting potential improvements.

Adversarial Attack: Adversarial attacks aim to generate adversarial examples that can fool the target model into predicting wrongly. The vulnerability of DNNs has sparked significant concerns in many safety-critical fields, including face recognition [29],

autonomous driving [58, 65] and human activity recognition [12]. Very recently, the adversarial attack against Deepfake detection has drawn attention. Hussain et al. [25] employ gradient sign-based methods [19, 34] to evaluate the adversarial robustness of video Deepfake detectors. Li et al. [35] generate adversarial fake images along the latent face manifold. Carlini et al. [3] and Neekhara et al. [44] investigate the adversarial threat to Deepfake detection under the black-box setting. Jia et al. [28] propose to generate adversarial perturbations in the frequency domain. Hou et al. [23] narrow the feature distribution gap between real and fake images by incorporating natural degradation noise with adversarial perturbations.

Different from Deepfake tampering the real face images, AI-generated image encompasses a broader range of synthetic images with more diverse semantic content, amplifying their potential for dissemination of disinformation. However, the adversarial robustness of AIGI detection has received little attention. In this paper, we propose a universal attack against both AIGI detectors and Deepfake detectors, and evaluate under the white-box and a more practical black-box setting.

3 METHODOLOGY

3.1 Preliminaries

Let \mathbf{x} and y represent the original image and its corresponding label. f_{Θ} denotes the AI-generated image detectors. We aim to inject adversarial perturbation into the original image that makes the detector misclassify. Such an adversary problem can be optimized by minimizing the predictive probability, i.e. maximizing the classification loss:

$$\arg \min_{\tilde{\mathbf{x}}} p(y | \tilde{\mathbf{x}}, \Theta) = \arg \max_{\tilde{\mathbf{x}}} L(\tilde{\mathbf{x}}, y, \Theta), \text{ s.t. } \|\delta\|_p \leq \epsilon \quad (1)$$

where L is the binary cross entropy loss in AI-generated image detection. Adversarial example $\tilde{\mathbf{x}} = \mathbf{x} + \delta$, in which δ is the adversarial perturbation and ϵ is the perturbation budget. Eq. (1) can be performed with iterative gradient-based methods, such as PGD [42] or I-FGSM [34]:

$$\tilde{\mathbf{x}}^{i+1} = \tilde{\mathbf{x}}^i + \alpha \cdot \text{sign}(\nabla L(\tilde{\mathbf{x}}^i, y, \Theta)) \quad (2)$$

$$= \tilde{\mathbf{x}}^i - \alpha \cdot \text{sign}(\nabla \log p(y | \tilde{\mathbf{x}}^i, \Theta)). \quad (3)$$

3.2 Frequency-based Analysis and Attacks

Many AIGI detection approaches distinguish between real and fake images via subtle artifacts [27, 55, 62]. While these subtle clues are invisible in the spatial domain, a series of works [5, 16, 17] demonstrate that there are obvious differences between real and fake images in the frequency domain. This inspires us to explore the vulnerable region of AIGI detectors from a frequency perspective. To this end, we first implement discrete cosine transform (DCT) $\mathcal{D}(\cdot)$ to transfer the inputs from the spatial domain to the frequency domain. To investigate the difference between real images and fake images in the frequency domain, we use the spectrum saliency map [40] to visualize the sensitive components of real and fake images across different models:

$$S_{\Theta} = \frac{\partial J(\mathcal{D}_{\mathcal{I}}(\mathcal{D}(\mathbf{x}), y, \Theta))}{\partial \mathcal{D}(\mathbf{x})} \quad (4)$$

where $\mathcal{D}_{\mathcal{I}}(\cdot)$ is the inverse discrete cosine transform (IDCT). In a spectrum map, the low-frequency components whose amplitudes are mainly distributed in the upper left corner, and the high-frequency components are located in the lower right corners. As shown in Fig. 3, (1) There are significant differences between synthetic images and real images in the frequency domain. Therefore, moving the image away from its original frequency distribution will make the detectors hardly classify it as the ground-truth class. This observation motivates us to attack under the frequency domain to push the original images away from their ground-truth frequency distribution. (2) Different models usually focus on different frequency components for classifying (Fig. 3(b~d)). This inspires us to conduct random spectrum transformation to stimulate diverse substitute models. Followed by [40], the spectrum transformation $\Gamma(\mathbf{x})$ is defined as:

$$\Gamma(\mathbf{x}) = \mathcal{D}_{\mathcal{I}}(\mathcal{D}(\mathbf{x} + \xi) \odot \mathcal{M}), \quad (5)$$

where $\Gamma(\cdot)$ denotes the random spectrum transformation [40]. \odot is the Hadamard product, ξ is a random noise drawn from an isotropic Gaussian $\mathcal{N}(0, \sigma^2 \mathbf{I})$, and each element of \mathcal{M} is sampled from a Uniform distribution $\mathcal{U}(1 - p, 1 + p)$. As shown in Fig. 3(a), tuning the spectrum saliency map can cover most of the other models. We hence conduct adversarial attack in the frequency domain via spectrum transformation:

$$\arg \min_{\tilde{\mathbf{x}}} p(y | \Gamma(\tilde{\mathbf{x}}), \Theta), \text{ s.t. } \|\delta\|_p \leq \epsilon \quad (6)$$

3.3 Exploring the Surrogate Posterior Space

Although tuning the spectrum transformation in Eq. (6) can simulate different substitute models with a homogeneous architecture [40], it shows limited transferability when applied to heterogeneous architectures, e.g. transferring adversarial examples across ViTs and CNNs. This motivates us to consider the frequency-based attack from a Bayesian perspective, i.e. exploring the full posterior distribution of the surrogate model to further narrow this gap between heterogeneous models. Therefore, we redefine Eq. (6) by minimizing the Bayesian posterior predictive distribution:

$$\begin{aligned} & \arg \min_{\tilde{\mathbf{x}}} p(y | \Gamma(\tilde{\mathbf{x}}), \mathcal{D}) \\ & = \arg \min_{\tilde{\mathbf{x}}} \mathbb{E}_{\Theta \sim p(\Theta | \mathcal{D})} p(y | \Gamma(\tilde{\mathbf{x}}), \Theta), \text{ s.t. } \|\delta\|_p \leq \epsilon \end{aligned} \quad (7)$$

where $p(\Theta | \mathcal{D}) \propto p(\mathcal{D} | \Theta)p(\Theta)$. \mathcal{D} is the dataset and $p(\Theta)$ is the prior of model weights. Attacking Bayesian Neural Networks (BNNs) rather than a single DNN allows for the output fusion from an ensemble of infinitely many DNNs with diverse predictions, thereby improving adversarial transferability.

3.3.1 Post-train Bayesian Strategy for Frequency-based Attack. However, it is not straightforward to attack AIGI detectors in such a Bayesian manner due to several factors. First, the Bayesian posterior for DNNs is a high dimensional distribution due to a very large number of parameters of DNNs [26]. Hence computing and sampling the posterior distribution is an intractable problem. Albeit feasible for approximate sampling the posterior via variational inference or Markov Chain Monte Carlo (MCMC), it is computationally slow and expensive in such a high dimensional space. Furthermore, to improve the accuracy and generalization of the AIGI detectors,

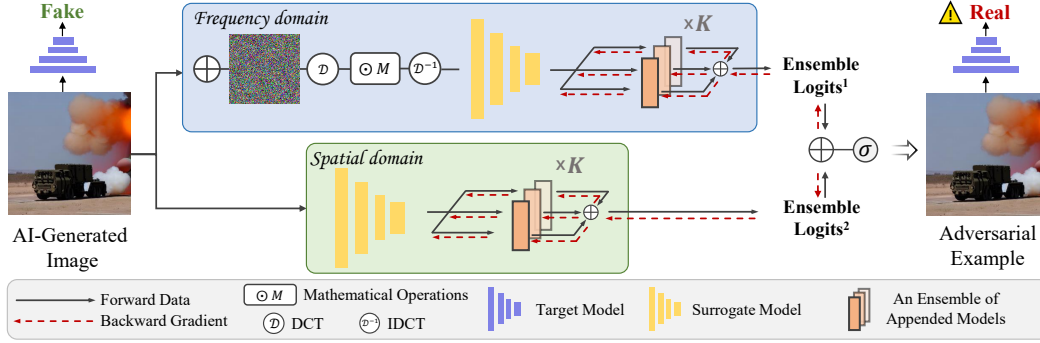


Figure 2: The workflow of FPBA. We add spatial-frequency adversarial perturbations to AI-generated images in a Bayesian manner, so that they are misclassified as real.

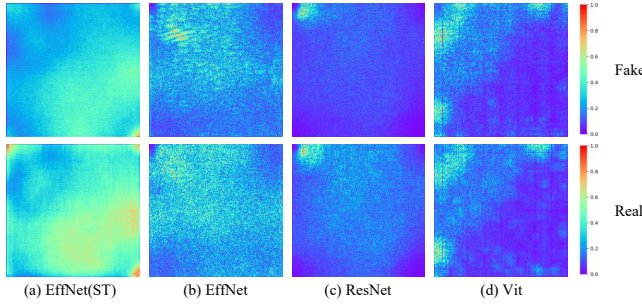


Figure 3: Visualization of the spectrum saliency map (average 2000 images on GenImage datasets) for real and fake images across different models. (a): the results for conducting frequency spectrum transformation ($N=10$). (b~d): the results for raw images on different models. The color value represents the absolute gradient value of the model loss function after max-min normalization.

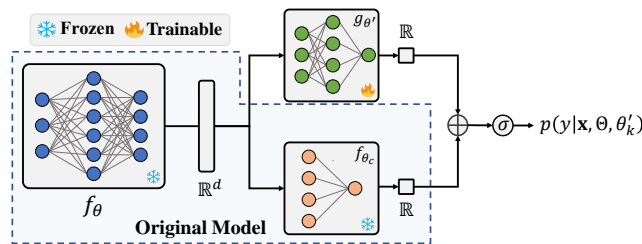


Figure 4: The architecture of the appended model. σ means the sigmoid layer.

there is a growing inclination to train AIGI detectors on large-scale datasets [21, 64]. From the perspective of end-users, it is not desirable to re-train a surrogate model on large-scale datasets for attack.

Therefore, we propose a *post-train* Bayesian strategy to turn a single surrogate into a Bayesian one, without the need for re-training. The parameters over the pre-trained surrogate are represented as $\Theta = [\theta, \theta_c]$, in which f_θ represents the feature extraction backbone,

and f_{θ_c} represents the fully-connected layer network for classification. As shown in Fig. 4, we fix the pre-trained surrogate and append a tiny Bayesian component $g_{\theta'}$ behind the feature extraction backbone f_θ . The new logits can be computed via a skip connection:

$$\text{logits} = g_{\theta'}(f_\theta(\mathbf{x})) + f_{\theta_c}(\mathbf{x}) \quad (8)$$

We choose to apply Bayesian Model Averaging to optimize the appended Bayesian model:

$$\mathbb{E}_{\theta' \sim p(\theta' | \mathcal{D}, \Theta)} p(y | \mathbf{x}, \Theta, \theta') \approx \frac{1}{K} \sum_{k=1}^K p(y | \mathbf{x}, \Theta, \theta'_k), \theta'_k \sim p(\theta' | \mathcal{D}, \Theta) \quad (9)$$

where K is the number of appended models. Θ is fixed to avoid re-training. We surprisingly find that adopting a simple MLP layer for appended models works well in all cases, hence training the appended models is much faster than re-training a surrogate. Finally, the frequency-based post-train Bayesian attack can be conducted with iterative gradient-based methods:

$$\tilde{\mathbf{x}}^{i+1} = \tilde{\mathbf{x}}^i - \alpha \cdot \text{sign} \left\{ \frac{1}{K} \sum_{k=1}^K \nabla \log p(y | \Gamma(\tilde{\mathbf{x}}^i), \Theta, \theta'_k) \right\} \quad (10)$$

3.3.2 Inference on Bayesian Appended Models. Θ is frozen after pre-training. We use Stochastic Gradient Adaptive Hamiltonian Monte Carlo[51] to sample appended model θ' in each iteration:

$$\begin{aligned} \theta'_{t+1} &= \theta'_t - \sigma^2 C_{\theta'_t}^{-1/2} \mathbf{h}_{\theta'_t} + \mathbf{N}(0, 2F\sigma^3 C_{\theta'_t}^{-1} - \sigma^4 \mathbf{I}) \\ C_{\theta'_t} &\leftarrow (1 - \tau^{-1}) C_{\theta'_t} + \tau^{-1} \mathbf{h}_{\theta'_t}^2 \end{aligned} \quad (11)$$

where σ represents the step size, F denotes the friction coefficient, \mathbf{h} is the stochastic gradient of the system, \mathbf{N} represents a Normal distribution, \mathbf{I} stands for an identity matrix, \mathbf{C} is a pre-conditioner updated through an exponential moving average, and τ is chosen automatically [51].

3.4 Hybrid Adversarial Attack

Despite detecting fingerprints fake images in the frequency domain, some works also extract fingerprint features in the spatial domain [27, 55]. We hence incorporate the attack gradient from the frequency domain with the spatial gradient to further improve the adversarial transferability across

Algorithm 1: Inference on FPBA

Input: \mathbf{x} : training data; N_{tra} : the number of training iterations;
 $M_{\theta'}$: sampling iterations for θ' ; Θ : parameters over pre-trained surrogate model; $\{\theta'_1, \dots, \theta'_K\}$: parameters over appended models;
 K : the number of appended models; ;
Output: The adversarial example $\tilde{\mathbf{x}}$;
// Post-train Bayesian Optimization
Randomly initialize $\{\theta'_1, \dots, \theta'_K\}$;
for $j = 1$ to N_{tra} **do**
 for $n = 1$ to K **do**
 Randomly sample a mini-batch data $\{\mathbf{x}, \mathbf{y}\}_j$;
 Compute $\mathbf{h}_{\theta'_k} = \frac{\partial \log p(\mathbf{y}|\mathbf{x}, \Theta, \theta'_k)}{\partial \theta'_k}$;
 for $t = 1$ to $M_{\theta'}$ **do**
 Update θ'_k with $\mathbf{h}_{\theta'_k}$ via Eq. (11);
 end
 end
end
return $\{\theta'_1, \dots, \theta'_K\}$;
// Frequency-based Post-train Bayesian Attack
 $\tilde{\mathbf{x}}^0 = \mathbf{x}$;
for $i = 1$ to I **do**
 for $n = 1$ to N **do**
 Get spectrum transformation output $\Gamma(\tilde{\mathbf{x}}^i)$ using Eq. (5) ;
 end
 for $k = 1$ to K **do**
 Averaging frequency gradient g_k using Eq. (13) ;
 Calculating spatial gradient d_k using Eq. (14) ;
 end
 Sample $\tilde{\mathbf{x}}^{i+1}$ from $\tilde{\mathbf{x}}^i$ via Eq. (12) ;
end
return $\tilde{\mathbf{x}}$;

different domains. Specifically, we define the hybrid attack as:

$$\tilde{\mathbf{x}}^{i+1} = \tilde{\mathbf{x}}^i - \alpha \cdot \text{sign} \left\{ \frac{1}{K} \sum_{k=1}^K (g_k^i + d_k^i) \right\} \quad (12)$$

$$g_k^i = \frac{1}{N} \sum_{n=1}^N \nabla \log p(\mathbf{y} | \Gamma(\tilde{\mathbf{x}}_{n-1}^i), \Theta, \theta'_k), \tilde{\mathbf{x}}_0^i = \tilde{\mathbf{x}}^i \quad (13)$$

$$d_k^i = \nabla \log p(\mathbf{y} | \tilde{\mathbf{x}}^i, \Theta, \theta'_k) \quad (14)$$

where g_k^i and d_k^i are the gradients computed in the frequency domain and spatial domain respectively. For frequency gradient, we conduct random spectrum transformation with N times to get more diverse spectrums. Our proposed method leverages both spatial attack gradients and frequency attack gradients in a Bayesian manner, aiming to further narrow the discrepancy between surrogate models and victim models. The complete algorithm of our method is presented in Algorithm 1. An overview illustration of FPBA is shown in Fig. 2.

4 EXPERIMENTS

4.1 Experimental Settings

Datasets: We choose three generated image datasets created by a wide range of generative models, across AIGI detection and Deepfake detection. Synthetic LSUN is a commonly used dataset proposed by CNNSpot [55], containing 720k real images from LSUN and 360k fake images generated by ProGAN [31]. GenImage [64] is a recently proposed large-scale dataset,

containing 1331k real images and 1350k fake images generated by eight generative models. Following the protocol in [64], we employ a subset of GenImage collecting 162k real images from Imagenet [10] and 162k Stable Diffusion(SD) V1.4 [49] generated images for training. The images generated by the other generators are used for testing in Sec. 4.3.2. To verify our proposed attack is a universal threat across AIGI and Deepfake detection, we also employ the synthetic FFHQ face dataset proposed by [50]. The Deepfake dataset consists of 50k real face images from FFHQ [32] and 50k generated face images generated by StyleGAN2 [32]. After training, we collect only the correctly classified testing samples for attack in evaluation.

Evaluated Models: We extensively evaluate the transferability of adversarial examples by eight different models across heterogeneous architectures under the spatial and frequency domain. We choose spatial-based classification models ResNet-50 [20] and MobileNet [24] as the source models. For target models, apart from the above models, we also use spatial-based models including EfficientNet [53], Vision Transformer(Vit) [14] and Swin-Transformer(Swin-Vit) [38], and frequency-based detectors DCTA [17] and Spec [60]. We report the accuracy of these detectors in the supplement. Besides, we also evaluate the robustness of state-of-the-art AIGI detection methods, including GramNet [39], LGrad [52], LNP [36] and UnivFD [45].

Compared Methods: We adopt gradient-based methods, I-FGSM [34], PGD [42], MI [13] and Frequency-based methods S²I [40]. We also consider ensemble-based methods Ensemble [13] and SVRE [59]. For a fair comparison, we ran 10 iterations with step size $\alpha = 2/255$ under l_∞ perturbation budget of 8/255 for all attacks.

Implementation Details: We choose classifiers pre-trained on ImageNet, and train them with Adam optimizer using Binary Cross-Entropy loss with an initial learning rate of 0.0001. We follow the same data augmentation strategy in CNNSpot [55]. Before cropping, images are blurred with $\sigma \sim \text{Uniform}[0, 3]$ with 10% probability, and JPEG-ed with 10% probability. We transformed images to 224 pixels and apply ImageNet normalization. For post-train Bayesian optimization, we follow the default setting in [54]. Although BNNs theoretically necessitate sampling numerous for inference, in practice, we find the number of models $K = 3$ is adequate. Opting for a larger number of appended models escalates computational overhead; thus, we opt for $K = 3$. For frequency-based attack, we set the tuning factor $\rho = 0.5$ for \mathcal{M} , the standard deviation σ of ξ is set to the value of ϵ , following [40]. All experiments were conducted on 4 NVIDIA GeForce RTX 3090s.

4.2 The Evaluation on Normally Trained Models

We show the attack performance against all models on all datasets in Tab. 1. Under the white-box setting, our proposed method FPBA achieves the highest attack success rate in all cases, and outperforms other competitive methods. Specifically, FPBA gets an average white-box success rate across different datasets and models as high as 99.8%, while S²I, PGD, IFGSM and MIFGSM only have 95.6%, 95.4%, 65.4% and 65.5%. Under the black-box setting, FPBA still achieves the highest average transfer success rate of 55.3%, surpassing MIFGSM, PGD and S²I by a margin of 27.7%, 7.6% and 8.4% respectively.

Next, We find that the attack results for FPBA are usually not the best on frequency-based models. To further investigate the reason, we plot the spectrum saliency map of frequency-based detectors using Eq. (4) in Fig. 5. Unlike spatial-based detectors, which rely on numerous frequency components to make decisions (see Fig. 3), the frequency components focused on in frequency-based models are very sparse. Therefore, the gradient information available from the spatial domain is much richer compared to the frequency domain. Nevertheless, our method still has the best average success rate over all models. In addition, we combine spatial-based gradient and frequency-based to further improve the attack performance on frequency-based models. FPBA gets an average transfer success rate of 43.1% against frequency-based detectors, which is only slightly lower 1.5%

Table 1: The attack success rate(%) on CNN-based, Vit-based and Frequency-based models on the Synthetic LSUN, GenImage subset and Synthetic FFHQ datasets. "Average" was calculated as the average transfer success rate over all victim models except for the surrogate model.

	Surrogate Model	Attack Methods	ResNet	DenNet	EffNet	MobNet	Spec	DCTA	ViT	Swin	Average
LSUN (ProGAN)	ResNet	IFGSM	52.1	51.3	24.6	48.4	17.7	48.0	35.2	46.2	38.7
		MIFGSM	52.1	51.5	27.9	47.6	26.1	49.8	37.5	42.7	40.4
		PGD	78.3	77.6	49.4	73	25.6	47.6	41.0	70.2	54.9
		S ² I	97.8	86.4	61.5	78.6	20.5	40.8	11.7	74.5	53.4
		FPBA(Ours)	98.9	98.0	76.4	95.9	19.8	48	51.5	94.8	69.2
	MobileNet	IFGSM	14.3	17.8	22.4	75.4	17.2	34.9	9.2	18.4	19.2
		MIFGSM	23.8	23.9	28.6	75.4	19.6	42	15.5	24.8	25.5
		PGD	20.3	26.0	20.6	97.6	25.0	40.4	9.7	29.9	24.6
		S ² I	14.4	17.5	34.7	97.8	16.3	25.4	4.3	14.6	18.2
		FPBA(Ours)	32.2	40.4	51.7	99.6	22.6	36.4	12.3	44.6	34.3
GenImage(SD)	ResNet-50	IFGSM	78.3	71.5	30.9	34.0	27.1	28.3	11.0	27.8	32.9
		MIFGSM	78.3	75.3	30.1	35.8	27.8	28.3	15.0	28.2	34.4
		PGD	99.3	88.0	48.5	52.2	48.6	49.9	15.4	48.1	50.1
		S ² I	98.0	91.0	66.8	64.7	36.7	50.1	16.9	53.0	54.2
		FPBA(Ours)	100	96.6	59.4	67.3	47.9	49.8	21.1	51.2	56.2
	MobileNet	IFGSM	9.0	8.9	8.9	58.9	9.1	9.1	4.4	8.5	8.3
		MIFGSM	9.7	9.2	8.9	59.0	9.5	9.0	5.9	8.8	8.7
		PGD	42.3	39.9	36.4	97.1	48.4	49.8	14.2	40.0	38.7
		S ² I	35.6	33.1	26.8	78.7	24.1	43.4	6.2	28.0	28.2
		FPBA(Ours)	49.7	46.8	44.0	100	44.1	49.4	16.6	45.0	42.2
FFHQ (Style GAN)	ResNet	IFGSM	67.5	67.5	55.3	67.5	28.9	32.5	16.2	17.5	40.8
		MIFGSM	67.5	67.5	54.9	67.6	28.8	32.6	20.7	17.9	41.4
		PGD	100	100	88.6	99.9	49.9	50	40.7	50.0	68.4
		S ² I	100	100	77.7	90.1	46.7	52.9	37.6	55.8	65.8
		FPBA(Ours)	100	100	86.8	100	49.4	49.6	43.1	50.9	68.5
	MobileNet	IFGSM	10.7	12.7	23.8	60.4	24.5	28.4	7.3	10.2	16.8
		MIFGSM	10.3	12.6	23.2	60.4	25.4	28.7	9.1	10.2	17.1
		PGD	49.8	50.2	57.5	100	49.7	49.8	38.8	49.8	49.4
		S ² I	82.8	86.7	78.5	100	51.4	51.8	28.9	49.7	61.4
		FPBA(Ours)	51.2	55.2	66.6	100	50.3	49.9	39.4	49.8	51.8

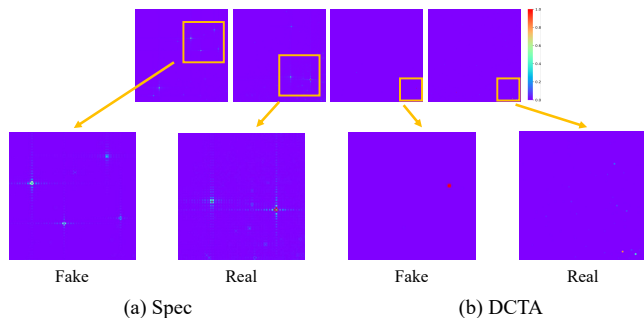


Figure 5: Visualization of the sensitive frequency components of real and fake images (average 1000 images on LSUN/ProGAN datasets) for frequency-based models. The frequency components of frequency-based models are highly sparse in comparison with spatial-based models.

than PGD, and much higher 3.3%, 15.8% and 17.6% than SSA, MIFGSM and IFGSM respectively.

Finally, FPBA has nearly top-2 results in all 48 cases (datasets vs. victim models vs. target models vs. attack setting), which shows consistent attack performance across different attack settings (white-box vs. black-box), tasks (AIGI detection vs. Deepfake detection) and models (CNN-based vs. Vit-based vs. Frequency-based detectors). We leave the detailed robustness analysis across models to Sec. 4.4.1.

Table 2: The attack success rate(%) compared with ensemble attack methods on Synthetic LSUN datasets. ¹ means setting (1), i.e. taking an ensemble of ResNet-50, MobileNet, and EfficientNet; ² means setting (2), i.e. taking an ensemble of ResNet, MobileNet and ViT; ³ means setting (3), i.e. taking an ensemble of ResNet, DCTA and ViT. ⁴ means only using ResNet as surrogate model.

Attack	ResNet	DenNet	EffNet	MobNet	Spec	DCTA	ViT	Swin	Ave
ENS ¹	55.9	45.4	69.9	76.2	16.8	42.9	23.3	43.7	34.4
SVRE ¹	63.7	64.5	75.5	72.9	10.3	30.4	28.6	64.2	39.6
ENS ²	57.3	58.6	54.1	92.8	19.5	38.5	77.9	59.7	46.0
SVRE ²	77.7	77.9	76.4	97.8	13.9	33.6	70.1	78.1	56.0
ENS ³	9.7	6.3	4.8	10.1	37.0	72.9	20.6	5.5	12.7
SVRE ³	22.6	12.9	8.1	13.2	29.4	87.0	24.0	9.6	14.6
FPBA⁴	98.9	98.0	76.4	95.9	19.8	48.0	51.5	94.8	69.2

4.2.1 Comparison with Ensemble-based Attacks. Considering that FPBA attacks an ensemble of appended models, we thus compare it with state-of-the-art ensemble-based methods, including ENSEMBLE [13] and SVRE [59]. Since there are three types of models for AIGI detection (CNN-based vs. Vit-based vs. Frequency-based detectors), we hence conduct an ablation study for ENSEMBLE and SVRE to investigate their impacts in 3 settings, including (1) taking CNNs as ensemble surrogates (ResNet-50, MobileNet, EfficientNet); (2) taking CNNs and Vits as ensemble surrogates (ResNet-50, MobileNet, ViT); (3) taking CNNs, Vits and frequency-based detectors as ensemble surrogates (ResNet-50, DCTA, ViT). Although we can also use more than one architecture for our method, we only use ResNet-50

Table 3: Transfer-based attack against SOTA detectors on Synthetic LSUN (ProGAN) datasets. The surrogate model is chosen as CNNSpot [55].

Attack	GramNet	LGrad	LNP	UnivFD	Ave
IFGSM	39.4	7.5	37.0	14.6	24.6
MIFGSM	9.65	6.6	38.5	24.2	19.7
PGD	67.7	50.2	47.4	11.5	44.2
S ² I	49.1	49.1	28.3	8.3	33.7
FPBA	87.8	50.2	39.5	16.6	48.5

Table 4: Benign accuracy of models trained on SD V1.4 and evaluated on different generated data. ‘Real/Fake’ means the accuracy(%) on evaluating real/fake testing data.

Detector	Acc	Midj.	SDv1.4	SDv1.5	ADM	Wukong	BigGAN	Ave
Swin-ViT	All	60.5	100.0	99.9	50.8	99.7	50.0	76.8
	Real	100.0	100.0	100.0	100.0	100.0	99.9	100.0
	Fake	21.0	100.0	99.9	1.5	99.3	0.1	53.6
ResNet	All	62.0	99.6	99.5	50.3	97.9	49.8	76.5
	Real	99.4	99.6	99.6	99.5	99.6	99.4	99.5
	Fake	24.7	99.6	99.4	1.2	96.1	0.2	53.5
ViT	All	58.4	99.5	99.3	50.2	96.0	50.2	75.6
	Real	99.5	99.6	99.5	99.5	99.5	99.3	99.5
	Fake	17.4	99.3	99.1	0.9	92.4	1.1	51.7

as the surrogate architecture to verify the universal transferability across heterogeneous models. We report the results in Tab. 2. First, compared with setting (1), heterogeneous model ensemble in setting (2) enhances the transferability of ENSEMBLE and SVRE across ViT-based and CNN-based models, while a more comprehensive ensemble in setting (3) decreases the transferable performance except for the frequency-based detectors. We speculate that there are significant differences in the classification boundaries between frequency-based and spatial-based detectors, thus averaging the ensemble outputs might reduce the original attack strength crafted by a single surrogate. Second, FPBA solely on ResNet still achieves competitive results in comparison with ensemble methods. Somewhat surprisingly, the black-box results on FPBA even outperform white-box results on ENSEMBLE and SVRE in some cases. For instance, the adversarial example only generated by ResNet-50 with FPBA get success rate of 76.4% on EfficientNet, which is higher than ENSEMBLE¹ and SVRE¹ generated by an ensemble of ResNet-50, EfficientNet and MobileNet. This demonstrates our proposed method can approximate the true posterior distribution, in which different victim models can be sampled from the posterior.

4.3 The Evaluation on Diverse AIGI Detections

4.3.1 Attack SOTA AIGI Detectors. In this section, we examine the robustness of state-of-the-art (SOTA) AIGI detectors against adversarial attacks and present the results in Tab. 3. Even though these detectors can achieve SOTA detection performance on benign data, they still suffer from a serious adversarial threat and demonstrate our method is the strongest threat to these SOTA detectors. Unlike common detectors trained on the fake images for the task of binary classification, UnivFD [45] extract fixed features via CLIP [47] and use nearest neighbor or linear probing for classification. The obvious diversity of the surrogate model(CNNSpot) and victim model(UnivFD) leads to a limited adversarial transferability on each other. Nevertheless, our method still achieves the best results on UnivFD compared to other attacks.

4.3.2 Attack Cross-Generator Image Detection. One important real-world detection problem is cross-generator image detection, i.e. identifying fake images generated by unseen generative models. We hence evaluate the

Table 5: The attack success rate (ASR) of cross-generator image detection on different generated subsets. The surrogate model is chosen as Swin-ViT.

Victim	Midj.	SDv1.4	SDv1.5	ADM	Wukong	BigGAN	Ave
Swin-ViT	97.6	97.4	97.7	96.2	96.9	97.1	97.1
ResNet	22.9	44.2	44.8	5.0	44.9	6.2	28.0
ViT	19.9	14.5	16.6	3.3	20.1	2.1	12.7

Table 6: The attack success rate (ASR) is reported on real images and fake images respectively. The surrogate model is chosen as Swin-ViT.

Victim	ASR	Midj.	SDv1.4	SDv1.5	ADM	Wukong	BigGAN	Ave
Swin-ViT	Real	94.9	96.4	96.2	96.0	96.0	97.0	95.9
	Fake	96.5	98.3	98.7	100.0	97.9	100.0	98.3
ResNet	Real	3.0	3.4	2.9	2.0	3.6	4.6	3.2
	Fake	100.0	85.1	86.9	100.0	86.3	100.0	93.0
ViT	Real	0.1	0.0	0.3	0.3	0.4	0.4	0.3
	Fake	96.1	29.0	32.9	100.0	39.8	100.0	66.3

robustness of cross-generator image detection to investigate whether adversarial examples are a real threat to AIGI detection. We train the detectors on images generated by SD v1.4 [49] and assess their robustness against adversarial examples, in which the adversarial perturbations are added to the images generated by Midjourney [43], SD V1.4 [49], SD V1.5 [49], ADM [11], Wukong [57] and BigGAN [2]. Because Swin-ViT achieves the SOTA results on different subsets [64], we use it as the surrogate model.

The benign accuracy and attack performance on unseen source data are reported in Tab. 4 and Tab. 5 respectively. First, the attack under the white-box setting achieves almost 100% success rate. Second, the transfer success rate is positively correlated to the accuracy on unseen source data. The Midjourney, SD v1.4&v1.5 and Wukong subsets have relatively high accuracy, their corresponding transfer attack success is also relatively high. In contrast, the binary classification accuracy drops to 50% on ADM and BigGAN subsets, the corresponding adversarial transferability is also limited on them. By looking closely at the accuracy/ASR on real images and fake images(Tab. 4,Tab. 6), we find detectors fail to distinguish fake images on ADM and BigGAN, which means without a good gradient can be followed to misclassify the real image as fake label under the attack. Therefore, we suggest robustness evaluation of cross-generator image detection should be conducted on the test subset with high accuracy as evaluating on the low-accuracy subset is futile.

4.3.3 Attack Defense Models. Furthermore, we evaluate FPBA on attacking defense models. We first employ adversarial training [42] for evaluation, which is the most popular defense baseline. However, according to our preliminary experiments(reported in the supplementary material), the training process of adversarial training fails to converge, which shows adversarial training is not a reliable way for evaluating attacks on AIGI detection. Considering that AIGI detection typically [55] uses JPEG compression and Gaussian blurring as data preprocessing during training to improve their robustness, we follow the suggestions from [55, 64] to utilize Gaussian blurring and JPEG compression as a defense. As shown in Tab. 7, existing attack methods all suffer from performance degradation as the probability of using Gaussian blurring and JPEG compression increases during training, while FPBA still contains a high attack success rate, which validates its effectiveness.

4.4 Additional Performance Analysis

4.4.1 The Phenomenon of Gradient Masking in AIGI Detectors. In Tab. 1, we find that the attack results of MIFGSM are similar to IFGSM, and

Table 7: Defense models(Blur+JPEG) against adversarial attack on ProGAN Dataset. Blur+JPEG(0.1) and Blur+JPEG(0.5) represented that images are blurred and JPEG-ed with 10% and 50% probability respectively. We report the attack success rate(%).

	Swin-ViT	
	Blur+JPEG(0.1)	Blur+JPEG(0.5)
IFGSM	98.8	86.6(-12.2)
MIFGSM	98.3	92.7(-5.6)
PGD	99.3	87.3(-12)
SSA	100.0	80.9(-19.1)
FPBA	100.0	99.2(-0.5)

significantly lower than PGD, in contrast to the common belief that adversarial examples generated by momentum iterative methods have higher success rate [13]. It indicates the possibility of gradient masking [1]. To investigate whether AIGI detectors exist in gradient masking, we analyze the aggregated gradient convergence properties. We take the adversarial examples crafted by ResNet-50 on ProGAN as an example. For each plot, we randomly sample 500 adversarial examples generated by a specific attack to compute their expected loss gradients. Each dot shown in Fig. 6 represents a component of the expected loss gradient from each image, in which there are a total of 75k loss gradient components.

Most gradient components of adversarial examples generated by IFGSM (Fig. 6(a)) and MIFGSM (Fig. 6 (c)) tend to stabilize around zero, indicating the vanishing gradient leading to a limited transferability to IFGSM and MIFGSM. Because the only difference between IFGSM and PGD is that PGD randomly chooses the starting point within the l_∞ constraint, we apply random initialization to MIFGSM and find the value of gradient component increase (Fig. 6 (d)), w.r.t. the average success rate increasing from 40.4% to 58.6% (still lower 10.6% than ours). This analysis formally demonstrates the phenomenon of gradient masking in AIGI detectors. Therefore, we advocate for future work for attacks on AIGI detectors to employ randomized-based strategies to circumvent the effect of gradient masking. Our proposed method conducts the spectrum transformation in the frequency domain and hence is also effective for gradient masking.

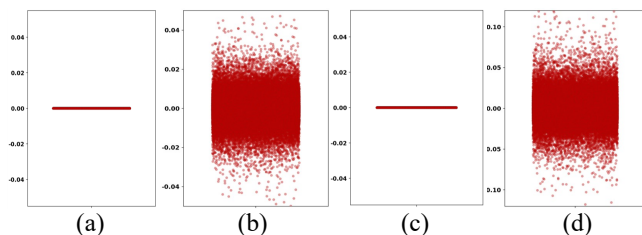


Figure 6: The gradient components of ResNet on adversarial examples generated by different attack methods. (a) gradient components of IFGSM; (b) gradient components of PGD; (c) gradient components of MIFGSM; (d) gradient components of MIFGSM with random initialization.

4.4.2 Qualitative Analysis. In this study, we evaluated the image quality of the generated adversarial samples using PSNR and SSIM scores as metrics. We present the quantitative results of MSE, PSNR(db) and SSIM in Tab. 8. The image quality of our method is higher than PGD. As illustrated in Fig. 7, FPBA can generate more natural-looking adversarial examples in comparison with PGD.

Table 8: The visual quality of different attack samples in terms of the average MSE, PSNR and SSIM scores.

Attack	MSE↓	PSNR(db)↑	SSIM↑
PGD	30.00	33.51	0.88
FPBA(Ours)	16.08	36.26	0.94

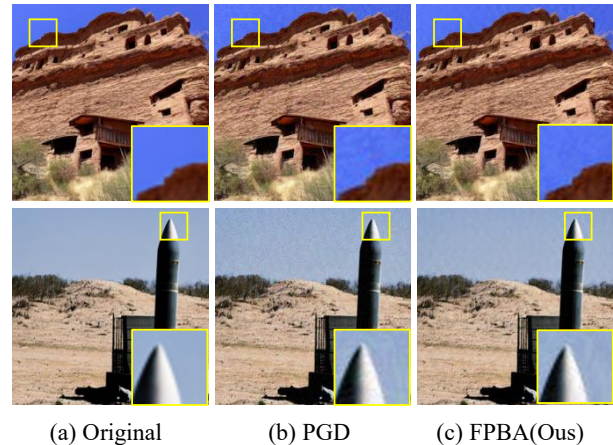


Figure 7: Visual comparison with PGD. (a): the original image generated by diffusion models. (b): adversarial examples crafted by PGD. (c): adversarial examples crafted by FPBA. The image quality of the adversarial example crafted by our method is much closer to the original image.

Table 9: Ablation Study on ProGAN dataset. The adversarial samples are crafted from ResNet50.

Attack	DenNet	MobNet	Spec	ViT
Spatial	71.5	34.0	27.1	11.0
Frequency	91.0	64.7	36.7	16.9
Spatial-frequency	96.2	66.2	47.9	21.0

4.4.3 Ablation Study. We conduct an ablation study in Tab. 9 to investigate the impact of computing gradient in different domains. In comparison with computing attack gradient solely in the spatial domain or frequency domain, our spatial-frequency attack achieves higher transferability. More ablation studies can be found in the supplementary material.

5 CONCLUSION

In this paper, we fully investigate the robustness of AIGI detectors against adversarial attacks. For the task of AIGI detection, we propose a novel frequency-based post-train Bayesian attack, which explores the vulnerable regions in the frequency domain in a Bayesian manner. More broadly, our proposed post-train Bayesian attack strategy extends the Bayesian attack family. Extensive experiments have been conducted across models, generators and defense methods under both white-box and black-box settings. The following conclusions can be drawn from our investigation.

- The current SOTA AIGI detectors are vulnerable to adversarial attacks, while the widely-used defense mechanism adversarial training cannot be directly applied to the AIGI detectors, which brings great challenges to build reliable and robust detectors.

- AIGI detectors rely on gradient masking to mitigate the transferability of gradient-based attacks, but the effect of gradient masking can be easily circumvented by a simple random initialization strategy.
- The attack success rate is positively associated with the detection accuracy. Therefore, evaluating detector robustness on low-accuracy subsets is futile, as there are no effective gradients for attack.

These findings indicate that building robust AIGI detectors is still an open problem. We hope that our work can be used as a protocol to evaluate the robustness of AIGI detectors and draw more attention to the robustness of AIGI detectors.

REFERENCES

- [1] Anish Athalye, Nicholas Carlini, and David Wagner. 2018. Obfuscated gradients give a false sense of security: Circumventing defenses to adversarial examples. In *International conference on machine learning*. PMLR, 274–283.
- [2] Andrew Brock, Jeff Donahue, and Karen Simonyan. 2018. Large Scale GAN Training for High Fidelity Natural Image Synthesis. In *International Conference on Learning Representations*.
- [3] Nicholas Carlini and Hany Farid. 2020. Evading deepfake-image detectors with white-and black-box attacks. In *Proceedings of the IEEE/CVF conference on computer vision and pattern recognition workshops*. 658–659.
- [4] Lucy Chai, David Bau, Ser-Nam Lim, and Phillip Isola. 2020. What makes fake images detectable? understanding properties that generalize. In *Computer Vision–ECCV 2020: 16th European Conference, Glasgow, UK, August 23–28, 2020, Proceedings, Part XXVI 16*. Springer, 103–120.
- [5] Keshigeyan Chandrasegaran, Ngoc-Trung Tran, and Ngai-Man Cheung. 2021. A closer look at fourier spectrum discrepancies for cnn-generated images detection. In *Proceedings of the IEEE/CVF conference on computer vision and pattern recognition*. 7200–7209.
- [6] You-Ming Chang, Chen Yeh, Wei-Chen Chiu, and Ning Yu. 2023. AntifakePrompt: Prompt-Tuned Vision-Language Models are Fake Image Detectors. *arXiv preprint arXiv:2310.17419* (2023).
- [7] Riccardo Corvi, Davide Cozzolino, Giovanni Poggi, Koki Nagano, and Luisa Verdoliva. 2023. Intriguing properties of synthetic images: from generative adversarial networks to diffusion models. In *Proceedings of the IEEE/CVF Conference on Computer Vision and Pattern Recognition*. 973–982.
- [8] Riccardo Corvi, Davide Cozzolino, Giada Zingarini, Giovanni Poggi, Koki Nagano, and Luisa Verdoliva. 2023. On the detection of synthetic images generated by diffusion models. In *ICASSP 2023–2023 IEEE International Conference on Acoustics, Speech and Signal Processing (ICASSP)*. IEEE, 1–5.
- [9] Davide Cozzolino, Giovanni Poggi, Riccardo Corvi, Matthias Nießner, and Luisa Verdoliva. 2023. Raising the Bar of AI-generated Image Detection with CLIP. *arXiv preprint arXiv:2312.00195* (2023).
- [10] Jia Deng, Wei Dong, Richard Socher, Li-Jia Li, Kai Li, and Li Fei-Fei. 2009. Imagenet: A large-scale hierarchical image database. In *2009 IEEE conference on computer vision and pattern recognition*. Ieee, 248–255.
- [11] Prafulla Dhariwal and Alexander Nichol. 2021. Diffusion models beat gans on image synthesis. *Advances in neural information processing systems* 34 (2021), 8780–8794.
- [12] Yunfeng Diao, Tianjia Shao, Yong-Liang Yang, Kun Zhou, and He Wang. 2021. BASAR: black-box attack on skeletal action recognition. In *Proceedings of the IEEE/CVF Conference on Computer Vision and Pattern Recognition*. 7597–7607.
- [13] Yinpeng Dong, Fangzhou Liao, Tianyu Pang, Hang Su, Jun Zhu, Xiaolin Hu, and Jianguo Li. 2018. Boosting adversarial attacks with momentum. In *Proceedings of the IEEE conference on computer vision and pattern recognition*. 9185–9193.
- [14] Alexey Dosovitskiy, Lucas Beyer, Alexander Kolesnikov, Dirk Weissenborn, Xi-aohua Zhai, Thomas Unterthiner, Mostafa Dehghani, Matthias Minderer, Georg Heigold, Sylvain Gelly, et al. 2020. An image is worth 16x16 words: Transformers for image recognition at scale. *arXiv preprint arXiv:2010.11929* (2020).
- [15] Ricard Durall, Margret Keuper, and Janis Keuper. 2020. Watch your up-convolution: Cnn based generative deep neural networks are failing to reproduce spectral distributions. In *Proceedings of the IEEE/CVF conference on computer vision and pattern recognition*. 7890–7899.
- [16] Tarik Dzanic, Karan Shah, and Freddie Witherden. 2020. Fourier spectrum discrepancies in deep network generated images. *Advances in neural information processing systems* 33 (2020), 3022–3032.
- [17] Joel Frank, Thorsten Eisenhofer, Lea Schönherr, Asja Fischer, Dorothea Kolossa, and Thorsten Holz. 2020. Leveraging frequency analysis for deep fake image recognition. In *International conference on machine learning*. PMLR, 3247–3258.
- [18] Ian Goodfellow, Jean Pouget-Abadie, Mehdi Mirza, Bing Xu, David Warde-Farley, Sherjil Ozair, Aaron Courville, and Yoshua Bengio. 2014. Generative adversarial nets. *Advances in neural information processing systems* 27 (2014).
- [19] Ian J Goodfellow, Jonathon Shlens, and Christian Szegedy. 2014. Explaining and harnessing adversarial examples. *arXiv preprint arXiv:1412.6572* (2014).
- [20] Kaiming He, Xiangyu Zhang, Shaoqing Ren, and Jian Sun. 2016. Deep residual learning for image recognition. In *Proceedings of the IEEE conference on computer vision and pattern recognition*. 770–778.
- [21] Yinan He, Bei Gan, Siyu Chen, Yichun Zhou, Guojun Yin, Luchuan Song, Lu Sheng, Jing Shao, and Ziwei Liu. 2021. ForgeryNet: A versatile benchmark for comprehensive forgery analysis. In *Proceedings of the IEEE/CVF conference on computer vision and pattern recognition*. 4360–4369.
- [22] Jonathan Ho, Ajay Jain, and Pieter Abbeel. 2020. Denoising diffusion probabilistic models. *Advances in neural information processing systems* 33 (2020), 6840–6851.
- [23] Yang Hou, Qing Guo, Yihao Huang, Xiaofei Xie, Lei Ma, and Jianjun Zhao. 2023. Evading DeepFake Detectors via Adversarial Statistical Consistency. In *Proceedings of the IEEE/CVF Conference on Computer Vision and Pattern Recognition*. 12271–12280.
- [24] Andrew G Howard, Menglong Zhu, Bo Chen, Dmitry Kalenichenko, Weijun Wang, Tobias Weyand, Marco Andreetto, and Hartwig Adam. 2017. Mobilenets: Efficient convolutional neural networks for mobile vision applications. *arXiv preprint arXiv:1704.04861* (2017).
- [25] Shehzeen Hussain, Paarth Neekhar, Malhar Jere, Farinaz Koushanfar, and Julian McAuley. 2021. Adversarial deepfakes: Evaluating vulnerability of deepfake detectors to adversarial examples. In *Proceedings of the IEEE/CVF winter conference on applications of computer vision*. 3348–3357.
- [26] Pavel Izmailov, Sharad Vikram, Matthew D Hoffman, and Andrew Gordon Gordon Wilson. 2021. What are Bayesian neural network posteriors really like?. In *International conference on machine learning*. PMLR, 4629–4640.
- [27] Yonghyun Jeong, Doyeon Kim, Youngmin Ro, Pyounggeon Kim, and Jongwon Choi. 2022. FingerprintNet: Synthesized fingerprints for generated image detection. In *European Conference on Computer Vision*. Springer, 76–94.
- [28] Shuai Jia, Chao Ma, Taiping Yao, Bangjie Yin, Shouhong Ding, and Xiaokang Yang. 2022. Exploring frequency adversarial attacks for face forgery detection. In *Proceedings of the IEEE/CVF Conference on Computer Vision and Pattern Recognition*. 4103–4112.
- [29] Shuai Jia, Bangjie Yin, Taiping Yao, Shouhong Ding, Chunhua Shen, Xiaokang Yang, and Chao Ma. 2022. Adv-attribute: Inconspicuous and transferable adversarial attack on face recognition. *Advances in Neural Information Processing Systems* 35 (2022), 34136–34147.
- [30] Yan Ju, Shan Jia, Jialing Cai, Haiying Guan, and Siwei Lyu. 2023. GIFF: Global and local feature fusion for ai-synthesized image detection. *IEEE Transactions on Multimedia* (2023).
- [31] Tero Karras, Timo Aila, Samuli Laine, and Jaakko Lehtinen. 2018. Progressive Growing of GANs for Improved Quality, Stability, and Variation. In *International Conference on Learning Representations*.
- [32] Tero Karras, Samuli Laine, and Timo Aila. 2019. A style-based generator architecture for generative adversarial networks. In *Proceedings of the IEEE/CVF conference on computer vision and pattern recognition*. 4401–4410.
- [33] Diederik P. Kingma and Max Welling. 2014. Auto-Encoding Variational Bayes. In *2nd International Conference on Learning Representations, ICLR 2014, Banff, AB, Canada, April 14–16, 2014, Conference Track Proceedings*, Yoshua Bengio and Yann LeCun (Eds.). <http://arxiv.org/abs/1312.6114>
- [34] Alexey Kurakin, Ian J Goodfellow, and Samy Bengio. 2018. Adversarial examples in the physical world. In *Artificial intelligence safety and security*. Chapman and Hall/CRC, 99–112.
- [35] Dongze Li, Wei Wang, Hongxing Fan, and Jing Dong. 2021. Exploring adversarial fake images on face manifold. In *Proceedings of the IEEE/CVF Conference on Computer Vision and Pattern Recognition*. 5789–5798.
- [36] Bo Liu, Fan Yang, Xiuli Bi, Bin Xiao, Weisheng Li, and Xinbo Gao. 2022. Detecting generated images by real images. In *European Conference on Computer Vision*. Springer, 95–110.
- [37] Huan Liu, Zichang Tan, Chuangchuan Tan, Yunchao Wei, Yao Zhao, and Jingdong Wang. 2023. Forgery-aware Adaptive Transformer for Generalizable Synthetic Image Detection. *arXiv preprint arXiv:2312.16649* (2023).
- [38] Ze Liu, Yutong Lin, Yue Cao, Han Hu, Yixuan Wei, Zheng Zhang, Stephen Lin, and Baining Guo. 2021. Swin transformer: Hierarchical vision transformer using shifted windows. In *Proceedings of the IEEE/CVF international conference on computer vision*. 10012–10022.
- [39] Zhengzhe Liu, Xiaojuan Qi, and Philip HS Torr. 2020. Global texture enhancement for fake face detection in the wild. In *Proceedings of the IEEE/CVF conference on computer vision and pattern recognition*. 8060–8069.
- [40] Yuyang Long, Qilong Zhang, Boheng Zeng, Lianli Gao, Xianglong Liu, Jian Zhang, and Jingkuan Song. 2022. Frequency domain model augmentation for adversarial attack. In *European Conference on Computer Vision*. Springer, 549–566.
- [41] Peter Lorenz, Ricard L Durall, and Janis Keuper. 2023. Detecting images generated by deep diffusion models using their local intrinsic dimensionality. In *Proceedings of the IEEE/CVF International Conference on Computer Vision*. 448–459.
- [42] Aleksander Madry, Aleksandar Makelov, Ludwig Schmidt, Dimitris Tsipras, and Adrian Vladu. 2017. Towards deep learning models resistant to adversarial attacks. *arXiv preprint arXiv:1706.06083* (2017).
- [43] Midjourney. 2022. <https://www.midjourney.com/home/>.

- [44] Paarth Neekhara, Brian Dolhansky, Joanna Bitton, and Cristian Canton Ferrer. 2021. Adversarial threats to deepfake detection: A practical perspective. In *Proceedings of the IEEE/CVF conference on computer vision and pattern recognition*. 923–932.
- [45] Utkarsh Ojha, Yuheng Li, and Yong Jae Lee. 2023. Towards universal fake image detectors that generalize across generative models. In *Proceedings of the IEEE/CVF Conference on Computer Vision and Pattern Recognition*. 24480–24489.
- [46] Orazio Pontorno, Luca Guarnera, and Sebastiano Battiato. 2024. On the Exploitation of DCT-Traces in the Generative-AI Domain. *arXiv preprint arXiv:2402.02209* (2024).
- [47] Alec Radford, Jong Wook Kim, Chris Hallacy, Aditya Ramesh, Gabriel Goh, Sandhini Agarwal, Girish Sastry, Amanda Askell, Pamela Mishkin, Jack Clark, et al. 2021. Learning transferable visual models from natural language supervision. In *International conference on machine learning*. PMLR, 8748–8763.
- [48] Jonas Ricker, Denis Lukovnikov, and Asja Fischer. 2024. AEROBLADE: Training-Free Detection of Latent Diffusion Images Using Autoencoder Reconstruction Error. *arXiv preprint arXiv:2401.17879* (2024).
- [49] Robin Rombach, Andreas Blattmann, Dominik Lorenz, Patrick Esser, and Björn Ommer. 2022. High-resolution image synthesis with latent diffusion models. In *Proceedings of the IEEE/CVF conference on computer vision and pattern recognition*. 10684–10695.
- [50] Fahad Shamshad, Koushik Srivatsan, and Karthik Nandakumar. 2023. Evading Forensic Classifiers with Attribute-Conditioned Adversarial Faces. In *Proceedings of the IEEE/CVF Conference on Computer Vision and Pattern Recognition*. 16469–16478.
- [51] Jost Tobias Springenberg, Aaron Klein, Stefan Falkner, and Frank Hutter. 2016. Bayesian optimization with robust Bayesian neural networks. *Advances in neural information processing systems* 29.
- [52] Chuangchuang Tan, Yao Zhao, Shikui Wei, Guanghua Gu, and Yunchao Wei. 2023. Learning on Gradients: Generalized Artifacts Representation for GAN-Generated Images Detection. In *Proceedings of the IEEE/CVF Conference on Computer Vision and Pattern Recognition*. 12105–12114.
- [53] Mingxing Tan and Quoc Le. 2019. Efficientnet: Rethinking model scaling for convolutional neural networks. In *International conference on machine learning*. PMLR, 6105–6114.
- [54] He Wang, Yunfeng Diao, Zichang Tan, and Guodong Guo. 2023. Defending black-box skeleton-based human activity classifiers. In *Proceedings of the AAAI Conference on Artificial Intelligence*, Vol. 37. 2546–2554.
- [55] Sheng-Yu Wang, Oliver Wang, Richard Zhang, Andrew Owens, and Alexei A Efros. 2020. CNN-generated images are surprisingly easy to spot... for now. In *Proceedings of the IEEE/CVF conference on computer vision and pattern recognition*. 8695–8704.
- [56] Zhendong Wang, Jianmin Bao, Wengang Zhou, Weilun Wang, Hezhen Hu, Hong Chen, and Houqiang Li. 2023. DIRE for Diffusion-Generated Image Detection. *arXiv preprint arXiv:2303.09295* (2023).
- [57] Wukong. 2022. <https://xihe.mindspore.cn/modelzoo/wukong>.
- [58] Shaoyuan Xie, Zichao Li, Zeyu Wang, and Cihang Xie. 2023. On the Adversarial Robustness of Camera-based 3D Object Detection. *Transactions on Machine Learning Research* (2023).
- [59] Yifeng Xiong, Jiadong Lin, Min Zhang, John E Hopcroft, and Kun He. 2022. Stochastic variance reduced ensemble adversarial attack for boosting the adversarial transferability. In *Proceedings of the IEEE/CVF conference on computer vision and pattern recognition*. 14983–14992.
- [60] Xu Zhang, Svebor Karaman, and Shih-Fu Chang. 2019. Detecting and simulating artifacts in gan fake images. In *2019 IEEE international workshop on information forensics and security (WIFS)*. IEEE, 1–6.
- [61] Yichi Zhang and Xiaogang Xu. 2023. Diffusion noise feature: Accurate and fast generated image detection. *arXiv preprint arXiv:2312.02625* (2023).
- [62] Nan Zhong, Yiran Xu, Zhenxing Qian, and Xinpeng Zhang. 2023. Rich and poor texture contrast: A simple yet effective approach for ai-generated image detection. *arXiv preprint arXiv:2311.12397* (2023).
- [63] Mingjian Zhu, Hanting Chen, Mouxiao Huang, Wei Li, Hailin Hu, Jie Hu, and Yunhe Wang. 2023. GenDet: Towards Good Generalizations for AI-Generated Image Detection. *arXiv preprint arXiv:2312.08880* (2023).
- [64] Mingjian Zhu, Hanting Chen, Qiangyu Yan, Xudong Huang, Guanyu Lin, Wei Li, Zhijun Tu, Hailin Hu, Jie Hu, and Yunhe Wang. 2024. Genimage: A million-scale benchmark for detecting ai-generated image. *Advances in Neural Information Processing Systems* 36 (2024).
- [65] Zijian Zhu, Yichi Zhang, Hai Chen, Yinpeng Dong, Shu Zhao, Wenbo Ding, Jiachen Zhong, and Shibao Zheng. 2023. Understanding the Robustness of 3D Object Detection With Bird's-Eye-View Representations in Autonomous Driving. In *Proceedings of the IEEE/CVF Conference on Computer Vision and Pattern Recognition*. 21600–21610.

Received 20 February 2007; revised 12 March 2009; accepted 5 June 2009